Journal of Manufacturing Processes 76 (2022) 796–811

Contents lists available at ScienceDirect

Journal of Manufacturing Processes

journal homepage: www.elsevier.com/locate/manpro

Grinding performance and theoretical analysis for a high volume fraction SiCp/Al composite

Peng Gu [a], Chuanmin Zhu [a,*], Andrea Mura [b,*], Giacomo Maculotti [c], Edoardo Goti [b]

[a] School of Mechanical Engineering, Tongji University, Shanghai 201804, China
[b] Department of Mechanical and Aerospace Engineering, Politecnico di Torino, Turin 10129, Turin, Italy
[c] Department of Management and Production Engineering, Politecnico di Torino, Turin 10129, Turin, Italy

ARTICLE INFO

Keywords:
SiCp/Al composite
Grinding
Friction and wear

ABSTRACT

SiCp/Al composite is widely used in space shuttle slides, automotive and machine tools. In this paper, ground surfaces of SiCp/Al composite, obtained with different grinding process parameters, are characterized in terms of friction and wear performances under dry and lubricated conditions. The wear mechanism of SiCp/Al composite is firstly found the combination of cohesive and abrasive wear, then a method to calculate the wear volume of SiCp/Al composite is proposed, and a comprehensive wear evaluation system of SiCp/Al composite is established, in which the three indicators of friction coefficient, wear depth, and equivalent wear section area are adopted to evaluate usability performance. The prediction models of the wear indicators were established and the errors between the experimental and predicted results are within 7%. Finally, the NSGA-II multi-objective algorithm is used to optimize surface performance of the SiCp/Al composite, and the optimized grinding process parameters are obtained as the wheel speed of 33 m/s, the table speed of 0.4 m/min and the grinding depth of 9 μm.

1. Introduction

Innovative materials are being developed to cope with the challenges of sustainability and increased components durability set by the current Industry 4.0 framework and environmental sustainability policies, *e.g.* the European Green Deal. Cermet, *i.e.* composites material with a metal matrix reinforced by ceramic particles, are one of the most appealing answers to these needs. They are employed both for final components and coatings to functionalize the surfaces by providing greater hardness and enhanced tribological properties [1]. Thought, they are hard-to-machine materials, which challenges grinding and finishing of the surface that is core to control their applications and tribological behavior [2]. Therefore, they require a thorough characterization [3].

SiCp/Al composite has the characteristics of high thermal expansion coefficient, low density and high hardness, and is widely used in the aerospace, military, automotive and machine tools. Surface topography has great influence on the friction and wear performance in dry conditions, which are becoming increasingly appealing to current industrial dry machining applications for sustainable processes adoption. It is meaningful to investigate the friction and wear performance of ground surface of SiCp/Al composite.

Many researchers have investigated the manufacturing process of the SiCp/Al composite. Yin G et al. [4] established the theoretical model of grinding force and the finite element simulation model of single diamond grain grinding of SiCp/Al composite. They concluded that the undeformed chip thickness (UCT) has a more significant influence on the machined surface quality. Liu J et al. [5] proposed a method to realize the ductile regime machining of the particle and divert away from the surface defects and improve the surface quality by selecting the cutting parameters in SiCp/Al composite micro-milling. Zhu C et al. [6] proposed the surface roughness prediction model and adopted the Rapid Non-dominated Sequencing Genetic Algorithm (NSGA-II) to optimize grinding process parameters of SiCp/Al composite considering grinding efficiency and surface roughness. Duan C et al. [7] proved that adding the minimum quantity of lubrication has good cooling, lubrication, and fluid flushing effects and is a better method for the machining of SiCp/Al composite. Zhou L et al. [8] highlighted the relevant role of the fracture model of silicon carbide particles on surface finishing and the edge quality. That work provides valuable information for a better understanding of the mechanics in the machining of the SiCp/Al composite. Zhou M et al. [9] carried out rotary ultrasonic grinding experiments of 45% volume fraction SiCp/Al composite to investigate grinding force,

* Corresponding authors.
E-mail addresses: 01065@tongji.edu.cn (C. Zhu), andrea.mura@polito.it (A. Mura).

https://doi.org/10.1016/j.jmapro.2022.02.051
Received 3 November 2021; Received in revised form 22 February 2022; Accepted 26 February 2022

surface quality, tool wear, and abrasive chip shapes. The related experimental results indicate that ultrasonic vibration could reduce grinding force, surface roughness, surface defects and increase the plastic removal ratio. Huang S et al. [10] found that the critical grinding depth of ductile-regime removal decreases with the increase of the tip radius of abrasive grains but increases with the decrease of the volume fraction of silicon carbide particles. Li J et al. [11] used SEM to analyze the formation mechanism of typical machined surface defects. They revealed that the simultaneous increase of cutting depth and feed velocity under the same change of material removal rate enables the adoption of lower mill-grinding force values.

The surface topography is related to the grinding parameters: when the feeding velocity and grinding depth are larger, the surface topography is more uneven. Yin G et al. [12] found that a common problem is the formation of voids and delamination on the machined surface in the grinding of SiCp/Al composite, which is due to reinforced particles pulling out and aluminum matrix adhesion on the machined surface. Zhou L et al. [13] indicated that cryogenic cooling is effective in enhancing the supporting function of the aluminum matrix to the silicon carbide particles and improving surface quality. Du J et al. [14] discussed the relevant removal modes and their mechanisms. The experimental results show that the aluminum matrix has larger plastic deformation, so the aluminum mixed with the surplus silicon carbide particles is cut from the surface. Zheng W et al. [15] developed a micromechanics finite element model to simulate the formation mechanisms of defects on the machined surface. They found that the cavity was the main defect on the machined surface. Chen Z et al. [16] showed that grinding damage can be prevented by silicon carbide particles, and a 60% volume fraction of silicon carbide particles can limit grinding depth. Liang G et al. [17] considered that the surface morphology can be evaluated in terms of the root mean square deviation of three-dimensional profiles, crushing ratio, and fractal dimension. Huang S et al. [18] observed the surface morphologies and chip shape after grinding through scanning electron microscope (SEM). They analyzed the chips chemical composition through energy density spectrometry (EDS) and the formation mechanism of different shape chips. Du J et al. [19] analyzed the removal mode of reinforced particle, aluminum matrix and their influence on the surface topography formation mechanism. They showed that, when the cutting speed increases, silicon carbide particles break or fracture, but the machined surface becomes smooth.

Furthermore, many researchers have investigated the wear mechanism. Ramachandra M et al. [20] carried out the microscopic examinations of the worn surfaces, wear debris, and subsurface of SiCp/Al composite. The results showed that the base alloy wear primarily due to the micro-cutting. Dimaki A et al. [21] used the FE method to investigate the influence of adhesive parameters of both external and internal surfaces on the wear. It showed that the wear regime changes from slipping to the brittle fracture of asperities with the increasing adhesion work. Huang J et al. [22] conducted friction experiments with copper-based composite materials and copper rings to study the friction properties of graphite/copper matrix composites. They found that wear was caused primarily by adhesion, abrasion, and oxidation in the process of mechanical wear without current-carrying. Rajeshkumar G et al. [23] adopted pin-on-disk wear testing machine to study the tribological performance of the fiber-reinforced composites based on epoxy. They showed that the presence of fibers in the composites improved the tribological performance. Wang Y [24] et al. prepared a metal matrix composite material mixed with alumina and silicon carbide particles by squeeze casting, it was found that as the content of silicon carbide particles increases at room temperature, the wear resistance decreases; when the temperature rises, the wear resistance of the SiCp/Al composite does not increase.

The literature review shows that, although extended research has been carried out in SiCp/Al composite, the wear mechanism of SiCp/Al composite compared with pure material is not clear, the wear performance and evaluation of SiCp/Al composite when finished under different grinding parameters need to be investigated more. In this paper, the grinding surfaces of SiCp/Al composite manufactured with different grinding process parameters are obtained, then the friction and wear tests are carried out under the dry and lubricated conditions. The wear mechanism of SiCp/Al composite is revealed, then a comprehensive evaluation system of SiCp/Al composite is established, the prediction models of wear indicators in the comprehensive evaluation system were drawn and verified. Finally, the grinding process parameters are optimized based on friction and wear performance of SiCp/Al composite.

2. Methodology

In order to investigate the grinding performance of SiCp/Al composite obtained with different grinding process parameters, the methodology is shown in Fig. 1, which includes five key points:

Firstly, the workpiece of SiCp/Al composite is ground with different grinding process parameters by grinding machine tool.

Secondly, the friction and wear tests of the ground surface are carried out under dry and lubricated conditions.

Thirdly, the friction and wear mechanism is investigated by SEM and EDS analysis.

Fourthly, a comprehensive evaluation system of SiCp/Al composite is established. Friction coefficient, wear depth, and equivalent wear section area are adopted to evaluate usability performance.

Fifthly, the prediction models of wear indicators are drawn and verified, the optimized grinding process parameters are obtained.

2.1. Experimental material

The SiCp/Al composite for the friction and wear experiments has been produced by Xi'an Chuangzheng New Material Co., Ltd. by die-casting process. The matrix is aluminum alloy A356.2. The reinforcement particles are silicon carbide particles, with a volume fraction of about 65%, and an average diameter of 60 μm. The density, thermal diffusivity, thermal conductivity and elastic modulus of the considered material are shown in Table 1. Fig. 2 shows the surface morphology of SiCp/Al composite; the size of the samples for grinding is 40 × 40 × 10 mm, cut by wire saw cutting.

2.2. Experimental apparatus

As shown in Fig. 3(a), a Schleifring grinder (Schleifring K—P36 Compact, Germany) was used to grind SiCp/Al composite. A resin diamond grinding wheel with the characteristics summarized in Table 2 was used.

After the workpieces of SiCp/Al composite are ground, the SEM (Hitachi, S-3400N, Japan) in Fig. 3(c) is used to observe and analyze the surface topography of SiCp/Al composite, the grinding surface is measured by the roughness instrument (Landtek, SRT-200, China), which is shown in Fig. 3(d). Friction properties have been measured by reciprocating ball on plate tests, carried on by an Anton Paar, TRB tribometer (Laboratory of Mechanics at Politecnico di Torino, Italy), shown in Fig. 3(b). A 10 mm alumina ball was used as counter-body to wear out the composite samples during friction tests. Friction tests were performed in dry and lubricated conditions. For the lubricated condition, Mobile Jet oil II was distributed evenly on the surface of the workpiece with the aid of a precision pipe, as much to cover the whole surface. This oil is used for airplane gearboxes; it is a combination of a highly stable synthetic base fluid and a unique chemical additive package.

After the friction test of alumina-SiCp/Al composite, the SEM (Hitachi, S-3400N, Japan) and EDS (EDAX, APOLLOX, USA) in Fig. 3(c) is used to observe and analyze the surface topography of SiCp/Al composite. For calculating the wear volume, surface topography measuring

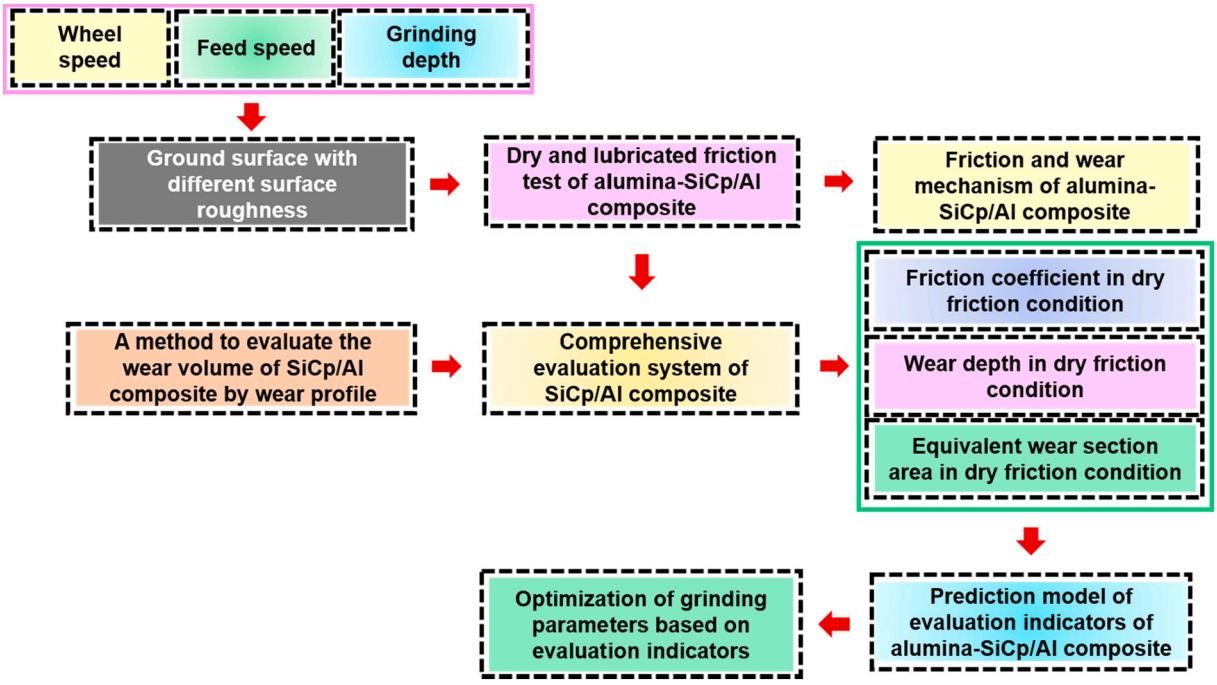

Fig. 1. Methodology of grinding performance of alumina-SiCp/Al composite.

Table 1
Material properties of SiCp/Al composite.

Parameter	Value
Thermal conductivity/W/(m·K)	226.4
Diffusivity/mm^2/s	90.105
Density/g/cm^3	2.97
Heat capacity/J/(g·K)	0.846
Elastic modulus/GPa	190

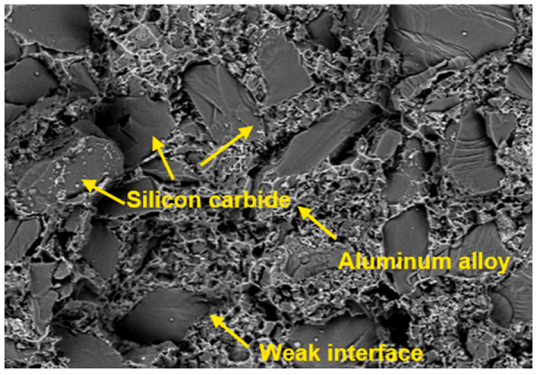

Fig. 2. Surface morphology of SiCp/Al composite.

instrument, *i.e.* optical topographical microscope, was used to measure the worn topography. The instrument used is a Zygo NewView 9000, a coherence scanning interferometry, shown in Fig. 3(e), hosted in the laboratory of Politecnico di Torino, Italy.

2.3. Experimental process

2.3.1. Grinding experiment

According to the design requirements of the center combination, the experimental program contains 3 factors and 3 levels. Let x_1 be the wheel speed v_s, x_2 be the feed speed v_w, and x_3 be the grinding depth a_p. The range of v_s is 15–35 m/s, the range of v_w is 0.3–0.9 m/min, and the range of a_p is 5–15 μm. Let s_{-1}, s_0, s_1 denote the −1, 0, and 1 levels of each processing variable, that are encoded as:

$$x_i = \frac{s_i - s_{0i}}{\Delta_i}, i = 1, 2, 3, \quad (1)$$

where x_i is the variable code, s_i is the machining variable parameter, s_{0i} is the 0 level of the grinding parameter variable, and Δ_i is the range of the current parameter. The coding table of grinding parameters is shown in Table 3:

The orthogonal response experiment design method was used based on Central Composite Surface Design (CCF): 15 groups of experiments were designed, as shown in Table 4.

2.3.2. Friction and wear test of SiCp/Al composite

As for the friction and wear test of SiCp/Al composite under different grinding process parameters, the total sliding distance was 2 m, the sliding frequency was 2 Hz, the amplitude oscillations 12 mm, the friction load was 5 N. Each sample was tested three times keeping the sliding direction always perpendicular to the grain direction. Both the friction ball and the sample surface were cleaned with the ethyl alcohol before tests. During the friction and wear test, the load was applied by dead weights placed on the pin, and the tangential friction force generated at the ball-sample interface was measured through an LVDT sensor sensing the displacement of a calibrated spring. The *a priori* vertical load knowledge allows calculating the friction coefficient as:

$$\mu = \frac{F_t}{F_n}. \quad (2)$$

The friction data are processed through the Tribological software to obtain the friction curves and average values. Bright filed observation under the optical microscope was exploited to analyze the worn region and explain the wear mechanisms. Finally, the surface topography of the worn regions were measured and the wear volume calculated based on the algorithm proposed in Section 4.

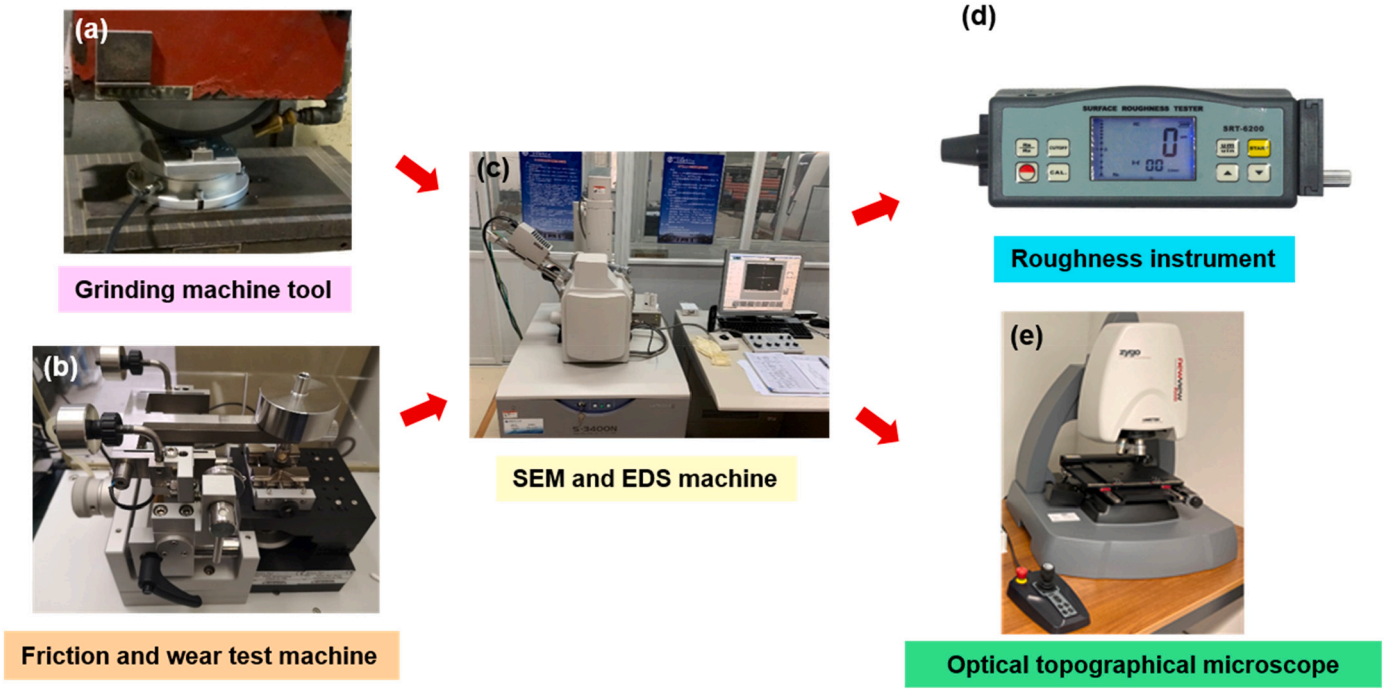

Fig. 3. Experimental apparatus of friction and wear test.

Table 2
Parameters of the grinding wheel.

Parameter	Value
Type	Resin diamond wheel
Diameter/mm	300
Thickness/mm	30
Concentration	100%
Diamond particle size	280#

Table 3
Coding table of grinding parameters.

Factor	Parameters and unit	Level		
		−1	0	1
A	Wheel speed v_s/m/s	15	25	35
B	Feed speed v_w/m/min	0.3	0.6	0.9
C	Grinding depth a_p/μm	5	10	15

Table 4
Grinding parameters of SiCp/Al composite.

No.	v_s/(m/s)	v_w/(m/min)	a_p/μm	x_1	x_2	x_3
1	15	0.9	15	−1	1	1
2	15	0.3	10	−1	−1	1
3	15	0.9	5	−1	1	−1
4	15	0.3	5	−1	−1	−1
5	15	0.6	10	−1	0	0
6	35	0.3	15	1	−1	1
7	35	0.9	15	1	1	1
8	35	0.6	10	1	0	0
9	35	0.9	5	1	1	−1
10	35	0.3	5	0	−1	−1
11	25	0.6	15	0	0	1
12	25	0.3	10	0	−1	0
13	25	0.9	10	0	1	0
14	25	0.6	5	0	0	−1
15	25	0.6	10	0	0	0

3. Friction and wear mechanism of SiCp/Al composite

3.1. Wear mechanism of SiCp/Al composite in dry friction test

A typical friction coefficient curve in the dry friction process ($v_s = 35$ m/s, $v_w = 0.3$ m/min, $a_p = 10$ μm) obtained by the software of the Anton Paar tribometer is shown in Fig. 4(a). The friction coefficient curve fluctuates greatly between positive and negative values because of the linear alternating motion. The maginified area shows that friction coefficient value fluctuates severely in the steady-state part of each stroke. As the frcition process continues, the ground surface will be more smooth, and the friction coefficient will decrease. The initial friction coefficient is closely related to the surface topography and adpoted as the friction coefficient in this paper.

Fig. 4(b) shows a typical worn surface of the alumina ball during the dry friction process against a SiCp/Al composite. The surface of the alumina ball is severely damaged during the dry friction test because of the strong abrasive action of the composite. The black matter inside the contact region is debris of the SiCp/Al composite welded onto the surface of the alumina ball. With the increase of friction time, wear on the surface of the alumina ball area gradually increases.

Fig. 5(a–b) shows friction surface of SiCp/Al composite at different magnifications under the optical microscope. Wear traces break original grinding lines on the sample surface with an irregular surface inside which cavities are visible corresponding to the silicon carbide particles expulsion sites. The elemental spectrum of the local area is analyzed by EDS (EDAX, APOLLOX, USA) in Fig. 5(b), as shown in Fig. 5(c). It can be found that silicon carbide particles are mostly in the wear area, and the content of Si element increased which further illustrates the debonding of silicon carbide and aluminum alloy.

Wear grooves aligned to the sliding directions are also visible inside the wear tracks, suggesting a dominating abrasive mechanism during the interaction. Abrasion is likely generated by the ploughing effect of both the hard sphere and the free silicon carbide particles at the contact interface. The black adhered material on the alumina ball is oxidized aluminum from the composite matrix due to the low hardness of the aluminum alloy and high hardness of alumina; when the alumina touches alumina, a cohesive mechanism is dominating. Therefore, the

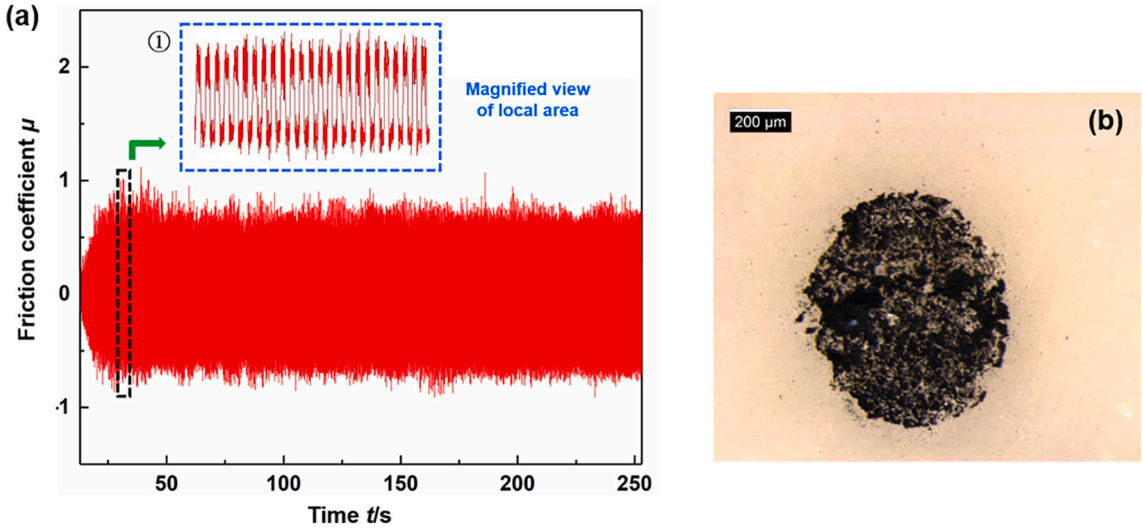

Fig. 4. Friction coefficient curve and worn surface of alumina ball in the dry friction process ((a) Friction coefficient curve (b) Worn surface on alumina ball).

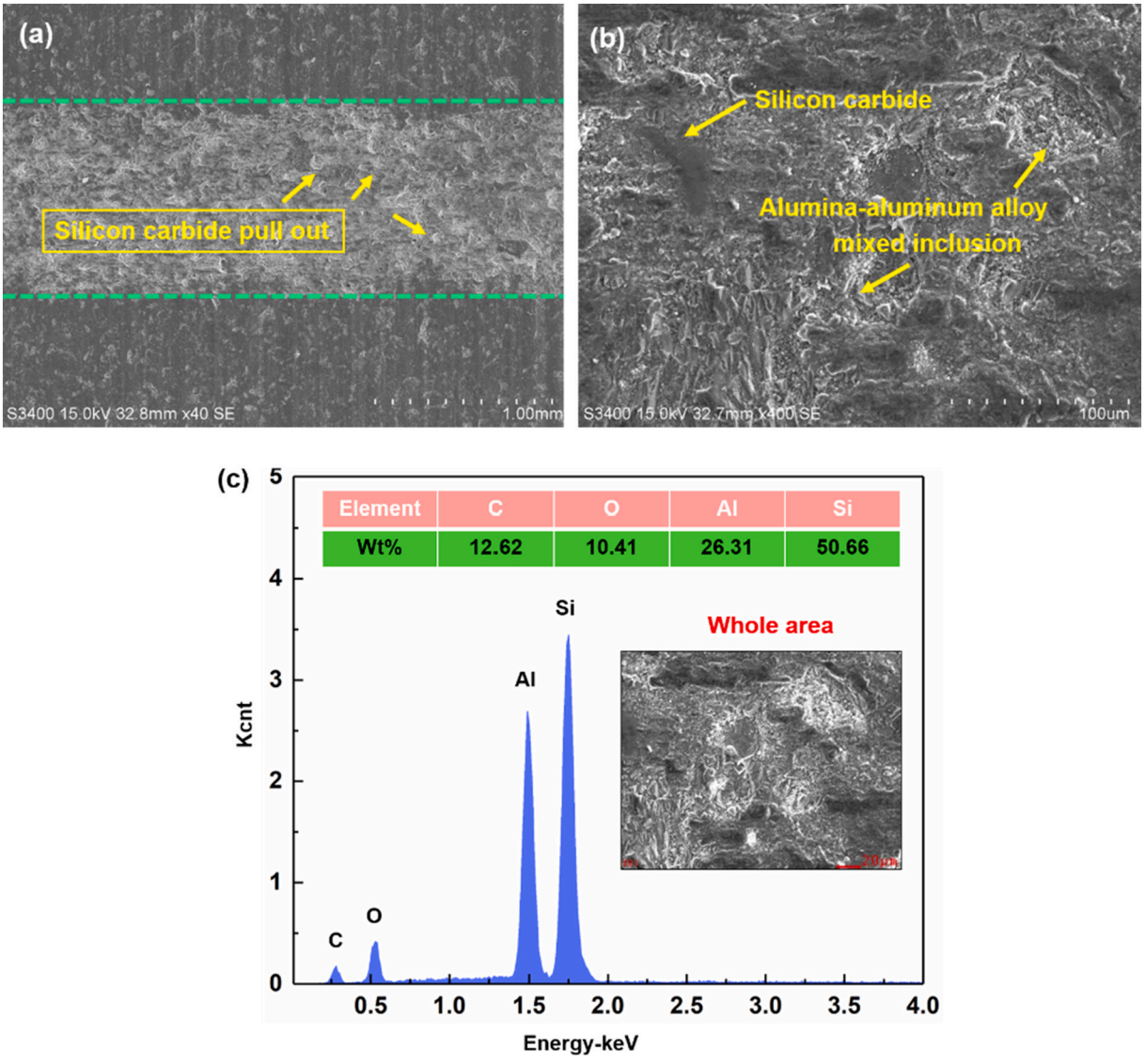

Fig. 5. Surface micromorphology of SiCp/Al composite in the dry friction process ((a)–(b) Surface wear morphology (c) Elemental analysis of local area in (b)).

wear mechanism of alumina-SiCp/Al composite is the combination of cohesive and abrasion mechanism.

3.2. Wear mechanism of SiCp/Al composite in lubricated friction test

Fig. 6(a) shows the friction coefficient curve of SiCp/Al composite in the lubrication friction process (v_s = 35 m/s, v_w = 0.3 m/min, a_p = 10 μm). In lubricated friction tests, the friction coefficient has a lower average steady state value during each stroke The area ① and ② in Fig. 6 (a) show that the friction curve has slightly lower fluctuations.

Fig. 6(b) shows a typical wear area on the alumina ball. Due to the presence of lubricating oil, the wear of the alumina ball is much less severe than that in dry conditions and, even though the size of the worn region is similar. However, compared with the dry friction condition, no welded debris on the ball surface is visible inside the contact region and the worn surface appeared smoother.

The following three interactions occur during the friction between the alumina ball and the workpiece: the furrowing of the rough peak, the adhesion of the rough peak, and the furrowing of the wear debris remaining on the surface. When the lubricating fluid fills the workpiece surface and the cavities, the wear debris remaining on the surface is taken away, the adhesion of the rough peaks is significantly reduced, and the furrowing effect of the rough peaks is basically dominated. In the process of furrowing with rough peaks, due to the characteristics of surface cavities, the interior of the cavities is soaked with lubricating fluid. During the friction process, the surface of the alumina can be kept coated with lubricating fluid, thereby reducing the furrows of rough peaks effect.

Fig. 7(a–b) shows the micromorphology of the friction surface of SiCp/Al composite. Due to the presence of lubricating oil, the surface wear of the SiCp/Al composite is significantly reduced compared with dry friction conditions. The elemental spectrum of the local area in Fig. 7 (b) is analyzed by EDS (EDAX, APOLLOX, USA), as shown in Fig. 7(e), (f), the elemental energy spectrum is similar to the elemental energy spectrum of the original SiCp/Al composite material. The silicon carbide particles are not significantly damaged, and the aluminum alloy is slightly damaged.

3.3. Comparison of wear mechanism of SiCp/Al composite in dry and lubricated friction test

Adhesive wear and abrasive wear are the most common wear type. The resulting topographies are particularly complex, and their quantitative characterization is challenging [3,25,26]. Abrasive wear is characterized by the presence of obvious scratches or furrows on the worn surface, and the worn debris is strips or chips. Conversely, surface generated by adhesive wear features fine scratches, significant material transfer, and wear debris are mostly flakes. The two relatively sliding surfaces undergo plastic strain under the action of friction, the surface oxide film is broken, the fresh metal surface is exposed to the surface, and the molecular force causes the surface to be welded.

If the external force is greater than the binding force, the external force will cause shear fracture [27]. Shearing occurs on the side with lower strength, while the metal surface with higher strength will adhere to the metal material on the opposite surface, and material transfer will occur. Some attachments can fall off the metal surface during repeated friction, forming wear debris.

In this work, the wear mechanism is going to be illustrated at the three wear stages considering microscopic change.

There are three wear stages for the friction process of alumina-SiCp/Al composite, namely, running-in stage, stable wear stage, and severe wear stage.

3.3.1. First stage: running-in stage

The alumina ball starts to touch with aluminum alloy and silicon carbide particles. In this stage, aluminum alloy starts to experience shear plastic deformation, silicon carbide particles start to generate crack.

3.3.2. Second stage: stable wear stage

The debris of aluminum alloy occurs and starts to adhere to the surface of alumina. The wear rate increases and aluminum alloy causes adhesive wear; some silicon carbide particles cause crack and cause abrasive wear. The cracks then expand under the high pressure, and some interfaces of aluminum alloy and silicon carbide particles start to fail.

3.3.3. Third stage: severe wear stage

With the increase of wear depth, the alumina ball adheres to aluminum alloy more severely. The friction area is enlarged, some silicon carbide particles are cracked while some are pushed outside the friction area, debris is generated in the whole friction process.

In the dry friction process, the wear rate increases from running in stage to severe wear stage, debris is generated in the whole friction process. In the lubricated friction process, due to the presence of lubricating oil, compared with dry friction conditions, there is no visible debris on the surface of the alumina ball in the contact area. The running in stage is very long; therefore, the wear of alumina ball and SiCp/Al composite is slight compared with that in the dry friction process.

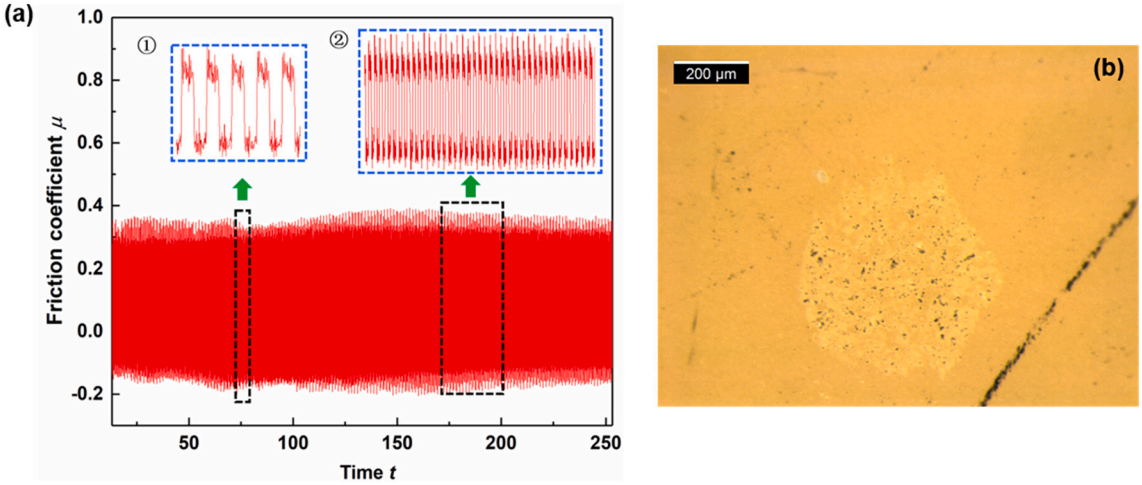

Fig. 6. Friction coefficient curve and worn surface of alumina ball in the lubricated friction process ((a) Friction coefficient curve (b) Worn surface on alumina ball).

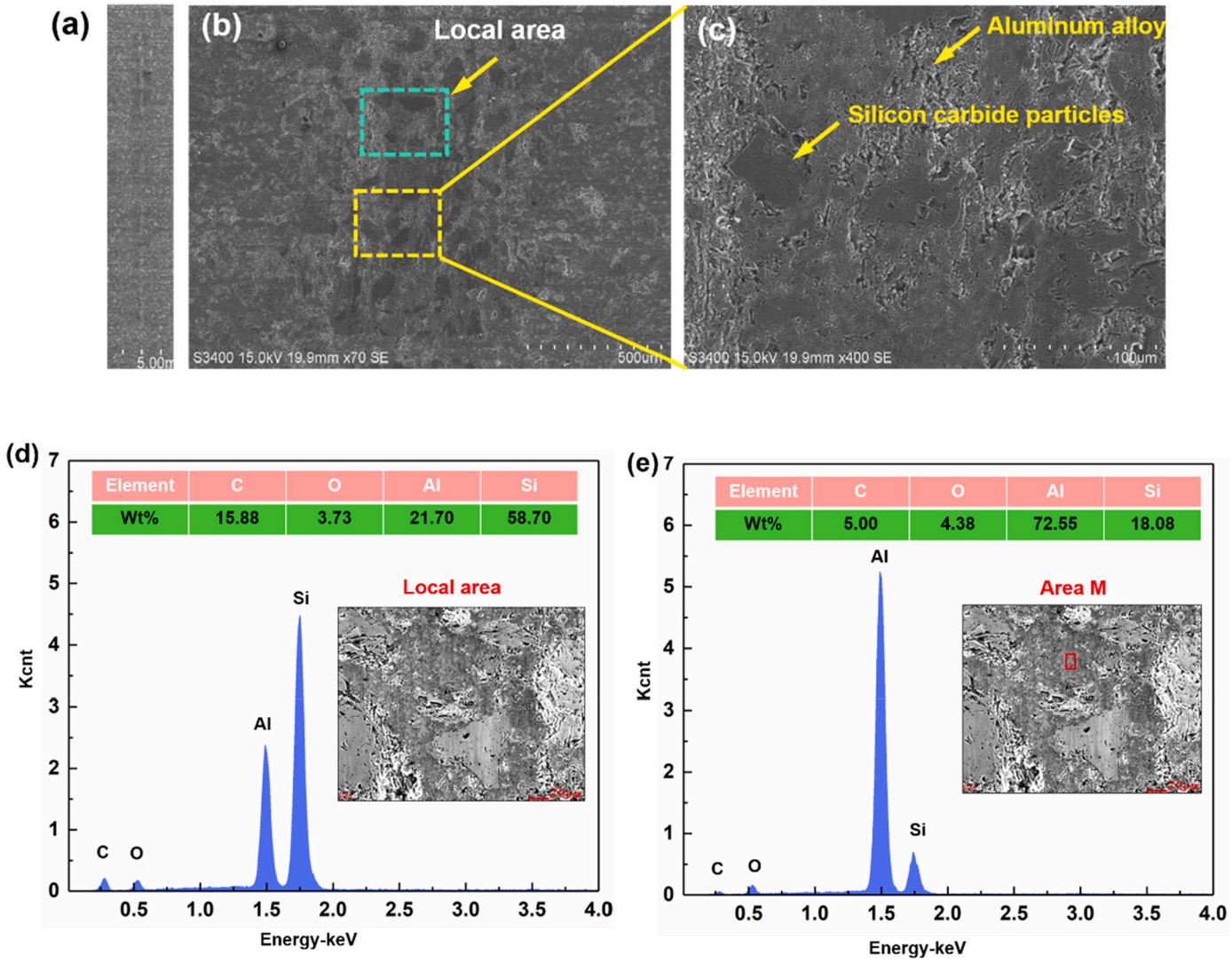

Fig. 7. Surface micromorphology and elemental analysis of SiCp/Al composite in the lubricated friction process ((a)–(c) Surface micromorphology (d)–(e) Elemental analysis of local area in (b)).

4. Evaluation method for wear volume of alumina ball and SiCp/Al composite

4.1. Surface topography reconstructed by point cloud

The bilinear interpolation algorithm was adopted to draw the contour map [28], to segment the point cloud measured by the surface topography measuring instrument Zygo NewView 9000 in the laboratory of Polytechnic of Turin. A diagram of the bilinear interpolation algorithm is provided in Fig. 8.

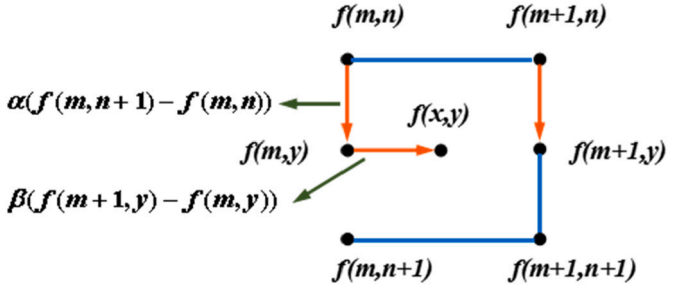

Fig. 8. Bilinear interpolation algorithm.

The value of $f(x,y)$ was calculated based on four neighboring points in the bilinear interpolation algorithm, and the coefficients α and β could be determined by Eq. (3):

$$\begin{cases} \alpha = x - m \\ \beta = y - n \end{cases}. \tag{3}$$

The value of $f(m,y)$ was calculated by the bilinear interpolation of $f(m,n)$ and $f(m,n+1)$ in Eq. (4):

$$f(m,y) = f(m,n) + \alpha[f(m,n) - f(m,n+1)]. \tag{4}$$

The value of $f(m+1,y)$ was calculated by the bilinear interpolation of $f(m+1,n)$ and $f(m+1,n+1)$ in Eq. (5):

$$f(m+1,y) = f(m+1,n) + \alpha[f(m+1,n) - f(m+1,n+1)]. \tag{5}$$

The value of $f(x,y)$ can be calculated by the bilinear interpolation of $f(m,y)$ and $f(m+1,y)$ in Eq. (6):

$$f(x,y) = f(m,y) + \beta[f(m+1,y) - f(m,y)]. \tag{6}$$

Therefore, Eq. (5) was substituted into Eq. (6), and Eq. (7) was obtained:

$$f(x,y) = f(m,y) + \beta[f(m+1,n) - f(m,n)] + \alpha\beta[f(m+1,n) + f(m,n+1) - f(m,n) - f(m+1,n+1)]. \tag{7}$$

For the grinding surface point cloud, the wear track surface topography could be segmented conveniently by means of the bilinear interpolation algorithm.

4.2. Closed contour area in contour map

The authors formerly proposed the comprehensive evaluation system of cavity features of the SiCp/Al composite [28], the surface cavity has the feature like a hole, which has small width and large length. In this research, the wear area has the feature of small length and large depth. The proposed algorithm is modified in this paper, and the specific process is as follows.

Fig. 9(a) illustrates an example of constructing a wear surface, Fig. 9 (b) illustrates the contour map of the wear surface. The surface topography has the similar feature of a cavity: a deep cavity at the center, and a gradually descending surrounding area.

The total length of the wear track is L, which is split into n parts, the contour corresponding to the length l_i is:

$$L_1 = \frac{L}{n}, L_2 = \frac{2L}{n}, \cdots, L_i = \frac{iL}{n}, L_n = \frac{nL}{n}. \tag{8}$$

Then, the assemble Q of the contour is:

$$Q = \{q(L_1), q(L_2), \cdots, q(L_n)\}, \tag{9}$$

where $q(l_1)$, $q(l_2)$, …, $q(l_n)$ are the contours corresponding to different lengths l_1,l_2, …,l_n, they have the similar shape with the rectangular.

Fig. 10(b) depicts one closed contour in the contour map of Fig. 10 (a), where A is the left point, B is the right point, C is the bottom point, F is the projection of A on the x axis, the abscissa of F is x_0, E is the projection of B on the x axis, and the abscissa of E is x_n. The upper part is the line AB, while the lower part is the line CD. The area S_1 is defined as equal to S_{ABEF}, the area S_2 is defined as equal to S_{ACDBEF}, and the closed contour area $S = S_{ACDB} = S_1 – S_2$. The calculation process of S is provided in Eq. (10):

$$S = \begin{matrix} \sum_{j=1}^{n}(x_{j+1} - x_j)(y_{j+1} + y_j) \Big/ 2 \\ -\sum_{i=1}^{n}(x_{i+1} - x_i)(y_{i+1} + y_i) \Big/ 2 \end{matrix}, \tag{10}$$

where x_i is the abscissa of the point on the upper curve AB, from x_0 to x_n, and x_j is the abscissa of the point on the lower curve ACDB, also from x_0 to x_n.

For the length L_i, the section contour corresponding to this length can be divided into k parts, the maximum of each wear height can be calculated. Then, the average value of section contour, corresponding to different lengths, can be considered as the wear height, and can be expressed as:

$$H = \frac{\sum_{i=1}^{n} Max(h_{i1}, h_{i2}, \ldots, h_{ik})}{n}. \tag{11}$$

The wear volume can be calculated based on the integration algorithm. The total wear volume V can be expressed as:

$$V = \sum_{i=1}^{n} S_i \Delta L. \tag{12}$$

When the n is large enough, the wear volume can be transformed into:

$$V = \int_0^L S_i dL. \tag{13}$$

Equivalent wear section area S is defined as the wear volume V divided by the friction length L:

$$S = \frac{V}{L}. \tag{14}$$

The Zygo NewView 9000 surface topography measuring instrument was used to collect the point cloud of the surface, then the point cloud was reconstructed by the bilinear algorithm. Fig. 11(a), (b) demonstrate the wear contour map of SiCp/Al composite and section view of wear topography when the wheel speed v_s is 35 m/s, the feed velocity v_w is 0.3 m/min, and the grinding depth a_p is 10 μm. The three wear tracks, corresponding to the replicated experiments, can be found in the point; the volume of each can be calculated according to the proposed algorithm.

Based on the above algorithm, the three indicators of friction coefficient, wear height, and equivalent wear section area can be obtained to indicate the wear degree of SiCp/Al composite.

5. Prediction model of wear indicators in friction process of alumina-SiCp/Al composite

In the following part, wear indicators for SiCp/Al composite surfaces, obtained with different grinding parameters, are investigated. Because it is difficult to obtain the wear height and section area of SiCp/Al composite in lubricated condition, which are too small, the relationship between wear indicators and grinding parameters in lubricated

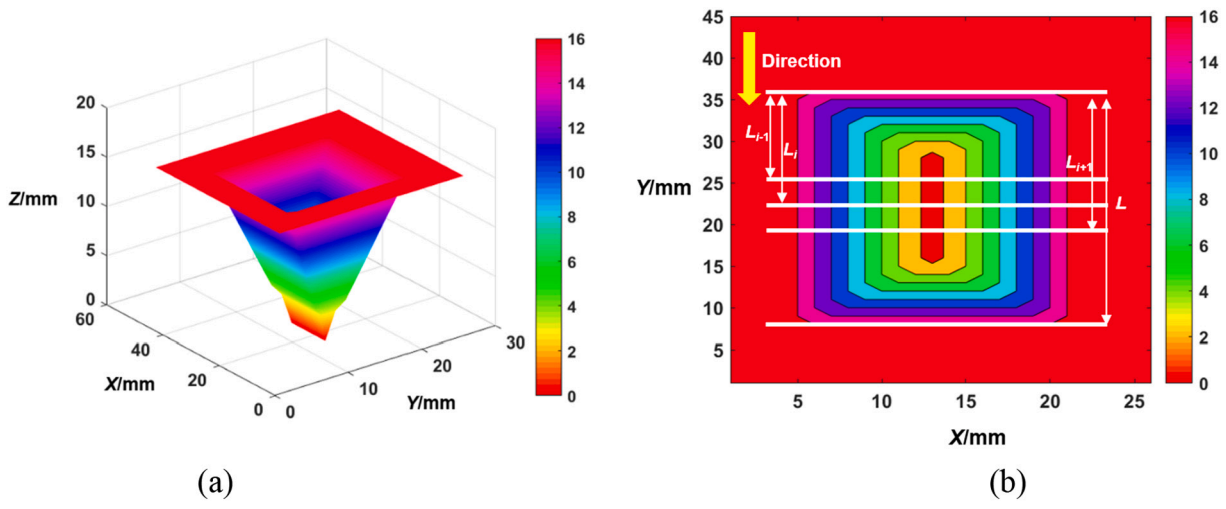

Fig. 9. Principal of constructing a wear surface ((a) An example of constructing a wear surface (b) Contour map of the wear surface in (a)).

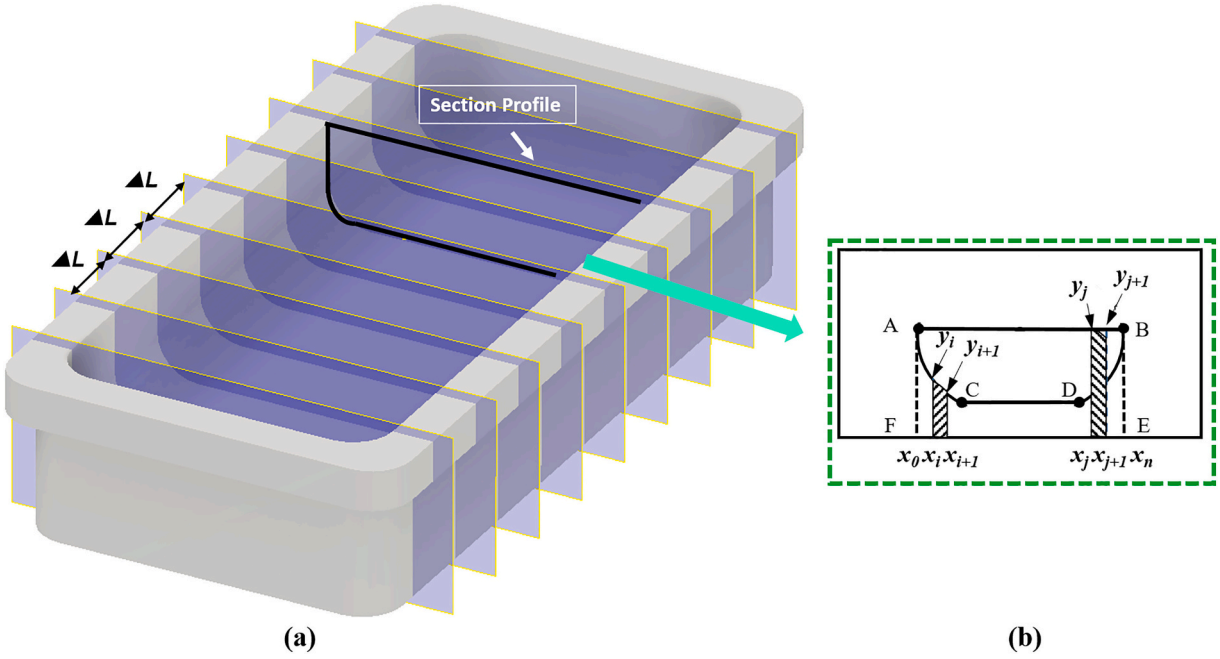

Fig. 10. Calculation process of area S ((a) An example of constructing a wear contour (b) One closed contour in (a)).

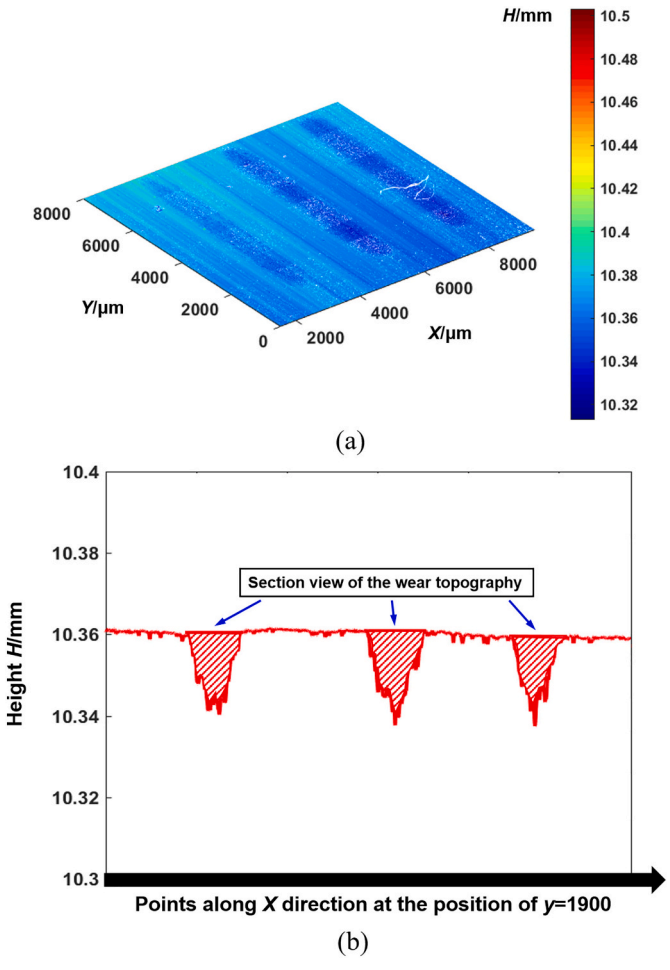

Fig. 11. Wear contour map and section view of SiCp/Al composite in dry friction process ((a) Wear contour map of SiCp/Al composite (b) Section view of wear topography in (a)).

condition is not obvious. Therefore, in this section, prediction model of wear indicators of alumina-SiCp/Al composite in dry friction process is established.

5.1. Wear indicators of alumina-SiCp/Al composite in dry friction process

Friction and wear performance is significant for the application guidance of SiCp/Al composite. The comprehensive evaluation system is important for the friction and wear performance of SiCp/Al composite. In fact, the traditional evaluation indicators like surface roughness, surface profile height cannot express usability adequately. A comprehensive evaluation system of SiCp/Al composite is proposed, in which friction coefficient, wear height, and equivalent wear section area are considered.

5.2. Friction and wear indicators of alumina-SiCp/Al composite in dry friction process

5.2.1. Friction coefficient of alumina-SiCp/Al composite in dry friction process

Response surface methodology is a statistical test method that relies on the design of experiment to explore the empirical relationship between continuous responses and (test) input factors [29]. It is often exploited to optimize manufacturing processes with respect to one or several responses [30].

Tribometer Demo 8.1.5 software was used to analyze and obtain the friction coefficient curve, whose absolute average was considered as friction coefficient. The least-squares estimation of each coefficient in the standard regression equation of the friction coefficient in the dry friction process is determined with the software Design Expert 8.0 in the Table 5, it can be found the p value of the quadric regression model is less than 0.0001, which means there is a significant relationship between the friction coefficient and grinding parameters.

Thus, a prediction model for the friction coefficient is established with wheel speed, feed velocity and grinding depth as variables:

$$\mu = 0.585 - 0.021v_s + 0.07v_w + 0.00149a_p + 0.0155v_w a_p + 0.00037v_s^2. \quad (15)$$

Table 5
Quadric regression model of friction coefficient μ in the dry friction process.

Model	Sum of squares	Mean square	Probability F value	p-Value
	0.091	0.018	50.04	<0.0001
v_s	4.813E-003	4.813E-003	13.21	0.0027
v_w	0.046	0.046	125.63	<0.0001
a_p	0.029	0.029	80.17	<0.0001
$v_w{}^*a_p$	4.340E-003	4.340E-003	11.92	0.0039
v_s^2	7.011E-003	7.011E-003	19.25	0.0006
Residual	5.099E-003	3.642E-004		
Lack of fit	3.928E-003	4.364E-004		
Cor total	0.096			

5.2.2. Wear height and section area of SiCp/Al composite in dry friction process

Wear height and equivalent wear section area are two important indicators to assess wear properties of the SiCp/Al composite. The least squares estimation of each coefficient in the standard regression equation of the wear height in the dry friction process is obtained using the software Design Expert 8.0 in the Table 6. It can be found the p-value of the whole model is less than 0.0001, which means there is a statistically significant relationship between the wear height H in the dry friction process and grinding parameters.

Thus, a prediction model of wear height H in the dry friction process is established in Eq. (16):

$$H = \begin{matrix} 18.98 + 0.367v_s - 0.259v_w + 0.329a_p - 0.015v_sv_w \\ -0.0139v_s^2 + 0.223v_sv_w^2 \end{matrix}. \quad (16)$$

Each coefficient in the standard regression equation of the equivalent wear section area S in the dry friction process is determined with the software Design Expert 8.0 in the Table 7, the p value of the quadric regression model is less than 0.0001, which means that the relationship between the equivalent wear section area S in the dry friction process and grinding parameters is significant.

Thus, a prediction model of equivalent wear section area S in the dry friction process is established in Eq. (17):

$$\begin{matrix} S = 5.389 - 0.126v_s - 0.035v_w - 0.182a_p + 0.00726v_sa_p \\ +0.211v_wa_p - 0.00649v_sv_wa_p + 0.00142v_s^2v_w - 0.00651v_sv_w^2. \end{matrix} \quad (17)$$

The residuals' normal probability plots of friction coefficient prediction model are shown in Fig. 12(a–b). The points are almost in a line; thus, it can be concluded that the prediction models of friction coefficient are suitable. Similar conclusions can be drawn for wear height and equivalent wear section area, from the residuals of the related prediction models that are shown in Fig. 12(c–d) and (e–f), respectively.

5.3. Validation of prediction model of wear indicators of alumina-SiCp/Al composite

Six experiments are conducted randomly to validate the prediction model of wear indicators. The grinding parameters of SiCp/Al composite are shown in the Table 8, and the experiments are conducted in the dry friction process.

Table 6
Quadric regression model of wear height H in the dry friction process.

Model	Sum of squares	Mean square	Probability F value	p-Value
	149.49	18.79	31.74	<0.0001
v_s	50.90	50.90	66.10	<0.0001
v_w	33.06	33.06	42.92	<0.0001
a_p	27.10	27.10	35.19	<0.0001
$v_s{}^*v_w$	4.60	4.60	5.97	0.0295
v_s^2	5.96	5.80	7.74	0.0155
$v_sv_w{}^2$	17.17	17.17	22.29	0.0004
Residual	10.01	0.77		
Lack of fit	10.01	1.25		
Cor total	156.68			

Table 7
Quadric regression model of equivalent wear section area S in the dry friction process.

Model	Sum of squares	Mean square	Probability F value	p-Value
	4.94	0.62	56.22	<0.0001
v_s	0.11	0.11	10.06	0.0089
v_w	0.093	0.093	8.44	0.0143
a_p	0.21	0.21	19.32	0.0011
$v_s{}^*a_p$	0.23	0.23	20.64	0.0008
$v_w{}^*a_p$	0.043	0.043	3.92	0.0734
$v_s{}^*v_w{}^*a_p$	0.060	0.060	5.47	0.0392
$v_s^2\,v_w$	0.068	0.068	6.16	0.0305
$v_sv_w{}^2$	0.20	0.20	18.28	0.0013
Residual	0.12	0.020		
Lack of fit	0.12	0		
Cor total	5.06			

The wear indicators of surface roughness, friction coefficient, wear height and equivalent wear section area are calculated and compared with the prediction of the related models obtained in Section 4.1 (see Fig. 13). The absolute error between the predicted and experimental results is within 7%, which proves that the prediction model of wear indicators of SiCp/Al composite is feasible [31], and can be applied in the actual prediction of wear indicators in the industry.

5.4. Influence of grinding process parameters of SiCp/Al composite on wear indicators of SiCp/Al composite

5.4.1. Influence of grinding process parameters on friction coefficient in dry and lubricated friction process

The broken line in Fig. 14(a–c) shows the influence of grinding process parameters on the friction coefficient in dry friction process, the surface friction coefficient of SiCp/Al composite grinding increases with the increase of the feed speed and grinding depth, but decrease with the increase of the wheel speed.

Generally speaking, the correlation between the friction coefficient and the wheel speed is less than the grinding depth and the feed speed. When the grinding wheel speed range is between 15 and 35 m/s, the feed speed range is 0.3–0.9 m/min, the grinding depth is between 5 and 15 μm, the SiCp/Al composite grinding surface has different degrees of cavities characteristics. Due to the cavities characteristics, the friction coefficient is increased during the dry friction process, and the wear of SiCp/Al composite and alumina pellets worsens.

The bar graph in Fig. 14(a–c) shows the influence of grinding process parameters on the friction coefficient under lubricating friction conditions. It can be found that the friction coefficient in the dry friction process is greater than the friction coefficient in the lubrication friction process, and the relationship between the friction coefficient and the grinding process parameters in the lubrication process is different from that in the dry friction process.

When a lubrication is present, the cavity stores the lubricating fluid, and the contact friction coefficient between the cavity surface and the alumina surface is greatly reduced, thus reducing the process of the cavity being smoothed. On the other hand, during the lubricated friction process of the small ball, alumina sometimes contacts the SiCp/Al composite plane for regular friction, and sometimes performs unconventional friction with the concave surface. In the process of unconventional friction with cavity surface, the surface of almina ball can be coated with lubricating fluid once and once again by the lubricating fluid storing in the cavities, thus the friction coefficient is small, which can reduce the flatting process of cavity surface and conventional surface.

5.4.2. Influence of grinding process parameters on the wear height and equivalent wear cross-sectional area in dry and lubricated friction process

Fig. 15(a–c) shows the influence of grinding process parameters on

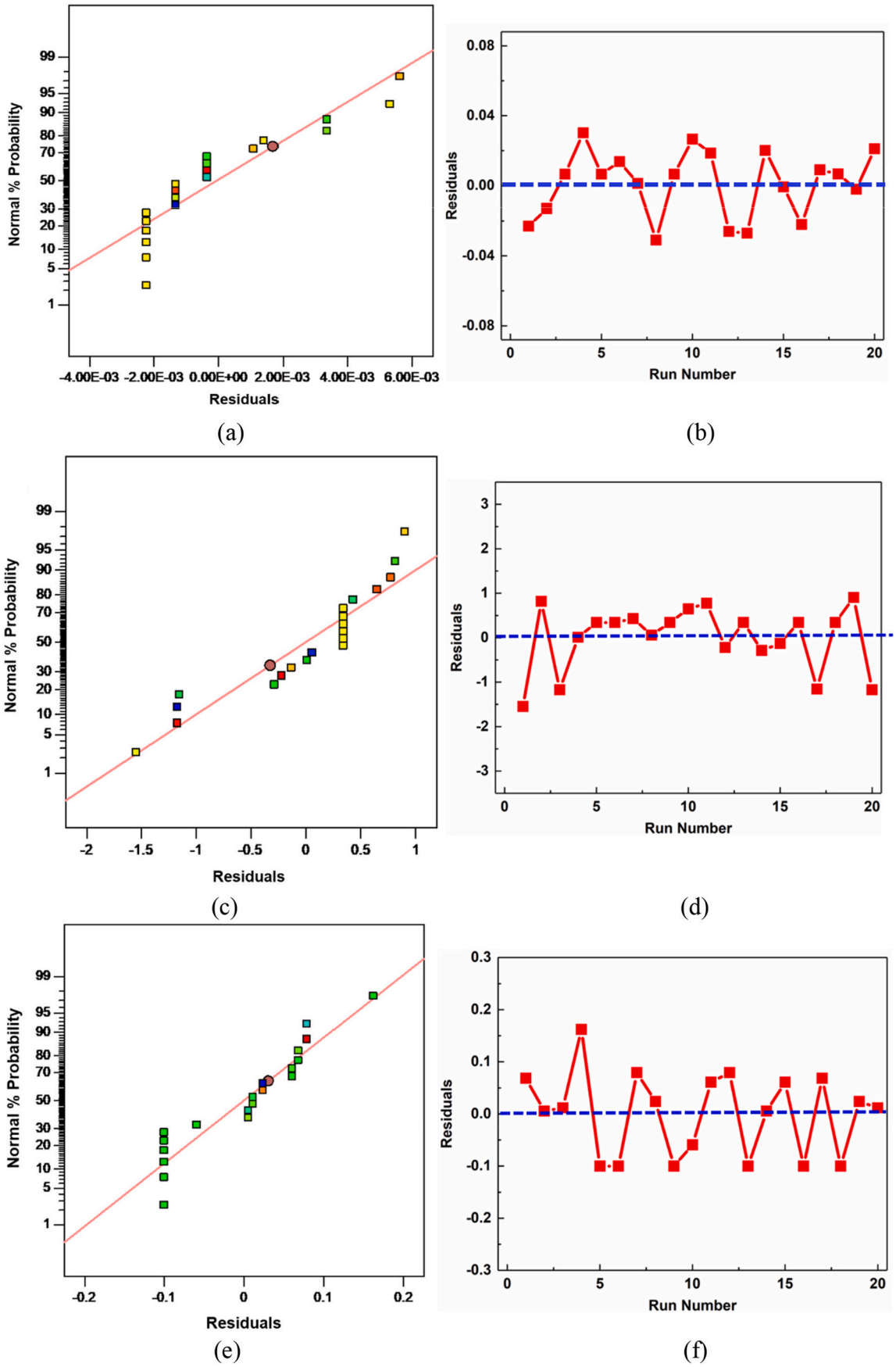

Fig. 12. Residuals of prediction model of (a–b) friction coefficient, (c–d) wear height and (e–f) equivalent wear section area.

Table 8
Grinding parameters of SiCp/Al composite.

No.	v_s/(m/s)	v_w/(m/min)	a_p/μm
1	15	0.4	15
2	35	0.7	12
3	25	0.9	8
4	15	0.3	6
5	25	0.6	6
6	35	0.8	5

the wear height and equivalent wear cross-sectional area in the dry friction process. The trend of the wear height and the equivalent wear cross-sectional area and the grinding process parameters is such that the equivalent wear section area increases with the increase of the feed speed and the grinding depth; the wear height and the equivalent wear section area do not change much.

The performance of SiCp/Al composite is of great significance for practical applications in industry. The correlation between the wear height and equivalent wear cross-sectional area of SiCp/Al composite and the grinding wheel speed is less than the grinding depth and the feed speed. When the grinding wheel speed ranges from 15 m/s to 35 m/s, the feed speed ranges from 0.3 m/min to 0.9 m/min, the grinding depth ranges from 5 μm to 15 μm, the grinding surface of SiCp/Al composite has different degrees of cavity characteristics. Due to the cavity characteristics, the frictional heat aggravates the wear of SiCp/Al composite and alumina pellets during the dry friction process. Then the cavities on the grinding surface of the SiCp/Al composite are gradually smoothed, the friction surface gradually becomes flat-curved.

Compared with dry friction process, the wear height and equivalent wear cross-sectional area of SiCp/Al composite in the lubricated friction process are significantly reduced. It is difficult to obtain the specific value. The relationship between wear indicators and grinding parameters in lubricated condition is not obvious. The grinding surface is prone to generate cavity features. Due to the cavity characteristics, the lubricating fluid can often be stored, which is beneficial to the friction performance improvement of the grinding surface. During the friction process, the friction coefficient of lubrication has been improved to a certain extent, which is conducive to reducing the wear degree.

Therefore, as for the lubricated friction process, the friction coefficients of grinding surfaces change not obviously when the grinding process parameters are within these ranges. As for the dry friction process, in the range of these grinding process parameters, the friction coefficients, the wear heights and equivalent wear cross-sectional areas of grinding surfaces change obviously, it is meaningful to optimize the grinding parameters based on wear indicators.

5.5. Optimization of grinding process parameters of SiCp/Al composite

5.5.1. Grinding parameters of SiCp/Al composite based on wear indicators

The NSGA-II algorithm was proposed on the basis of the non-dominated sorting genetic algorithm (NSGA) [32]. On the basis of the non-dominated sorting genetic algorithm (NSGA), it accelerates the non-dominated sorting process and introduces the concept of crowding degree operator. In addition, the core operator of the algorithm includes the elite selection operator. The basic core idea is to use the quick sorting operator to stratify the population. Then the crowding degree operator can be used to keep the excellent individuals until the next iteration, which greatly improves the algorithm speed and accuracy.

A vector $\bar{f}\left(\bar{X}\right) = \left(\bar{f}_1\left(\bar{X}\right), \bar{f}_2\left(\bar{X}\right), \cdots, \bar{f}_n\left(\bar{X}\right)\right)$ composed of N target components f_i ($i = 1,2,3, \ldots,n$), given two decision variables: $\bar{X}_u, \bar{X}_v \in U$.

If $\forall i \in \{1, \cdots, n\}$, $f_i\left(\bar{X}_u\right) . < f_i\left(\bar{X}_v\right)$, then $\bar{X}_u$ dominates $\bar{X}_v$;

If $\forall i \in \{1, \cdots, n\}$, $f_i\left(\bar{X}_u\right) \le f_i\left(\bar{X}_v\right)$, and at least one $j \in \{1, \cdots, n\}$, $f_i\left(\bar{X}_u\right) = f_i\left(\bar{X}_v\right)$, then $\bar{X}_u$ weakly dominates $\bar{X}_v$;

If $\exists i \in \{1, \cdots, n\}$, $f_i\left(\bar{X}_u\right) . < f_i\left(\bar{X}_v\right)$, $\exists j \in \{1, \cdots, n\} f_i\left(\bar{X}_u\right) . > f_i\left(\bar{X}_v\right)$, then $\bar{X}_u$ does not dominate $\bar{X}_v$;

If a solution $\bar{X}_u$ is a Pareto solution, no $\bar{X}_v \in U$ dominates $\bar{X}_u$.

The specific process of NSGA-II non-dominated sorting genetic algorithm is shown in Fig. 16, it includes three aspects:

(1) Initialize the population, generate N individuals according to the setting, and become the initial parent population, use the fast non-dominated operator to sort in the population;
(2) Calculate the degree of individual congestion, determine its level by the congestion degree, select the appropriate individual to put into the mating pool through the selection operator, perform operations such as crossover and mutation on the individual to generate the next generation of population;
(3) Repeat the above process with the obtained individual as the new parent through the elite selection operator, and finally, reach the termination condition.

5.5.2. TOPSIS decision method

In the process of multi-objective optimization, the optimal solution needs to be selected from the feasible solution set. The TOPSIS decision method is used to take such a decision on the Pareto optimal solution set in the NSGA-II algorithm. In the process of decision-making, different objectives need to be processed without reference to their dimensions, so

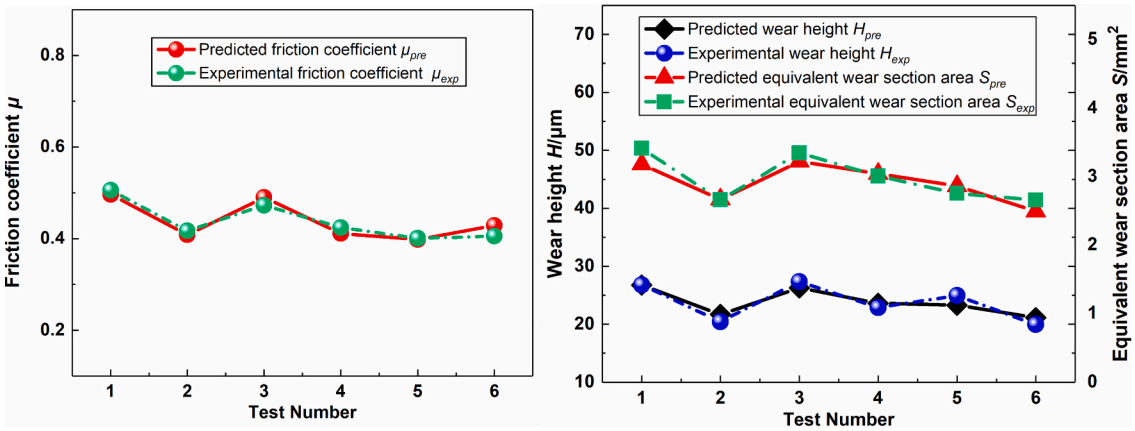

(a) Friction coefficient (b) Wear height and equivalent wear section area

Fig. 13. Comparison of experimental and predicted wear indicators.

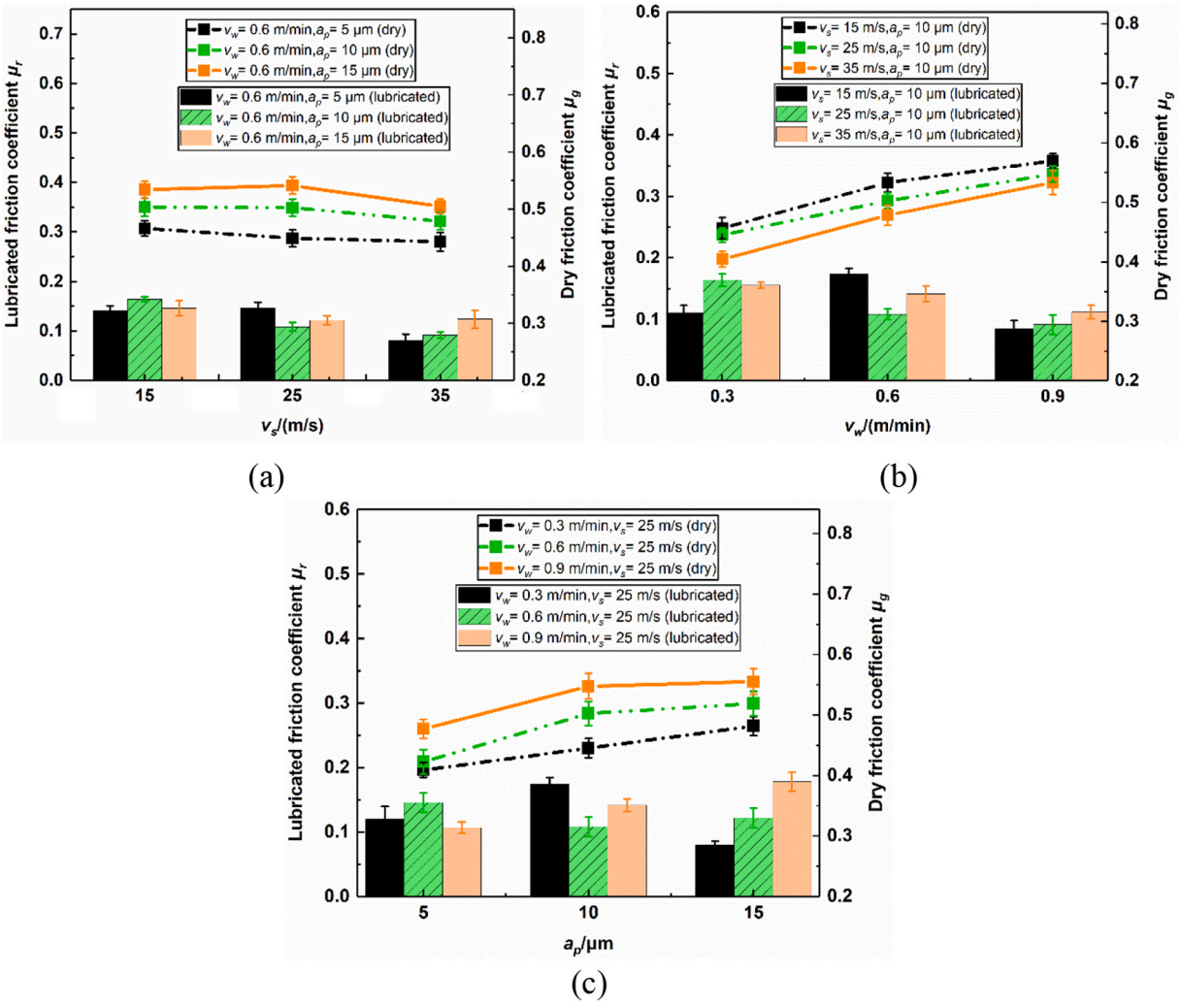

Fig. 14. Relationship between friction coefficient and grinding process parameters of SiCp/Al composite ((a) v_s and a_p (b) v_s and v_w (c) v_w and a_p).

that the dimensionality of the target space is unified [33].

The TOPSIS decision-making method adopts dimensionless method. The target matrix composed of points on the Pareto frontier is represented by f_{ij}, where i represents each point on the Pareto frontier, and j represents the dimension of the target space. Therefore, the target matrix is defined as:

$$f_{ij} = \frac{x_{ij}}{\sqrt{\sum_{i=1}^{m} x_{ij}^2}}, i = 1, 2, \ldots, m; j = 1, \ldots, n. \tag{18}$$

As shown in Fig. 17, in the TOPSIS decision-making process, the ideal point is that each objective function has reached the optimal value, and the non-ideal point is that each objective function has reached the worst value. In fact, the ideal point and the non-ideal point do not exist. The distances between each point on the Pareto front and both the ideal point and the non-ideal point are used as the selection criterion for the optimal solution:

$$d_{i+} = \sqrt{\sum_{j=1}^{n} \left(f_{ij} - f_j^i\right)^2}, \tag{19}$$

$$d_{i-} = \sqrt{\sum_{j=1}^{n} \left(f_{ij} - f_j^n\right)^2}, \tag{20}$$

where d_{i+} is the distance from each point on the Pareto front to the ideal point, d_{i-} is the distance from each point on the Pareto front to the non-ideal point, n is the number of objective functions, f_j^i is the optimal value of the j-th objective function under a single objective, f_j^n is the worst value of the j-th objective function under a single objective.

A comprehensive evaluation function Y_i is established:

$$Y_i = \frac{d_{i-}}{d_{i+} + d_{i-}}. \tag{21}$$

The solution that minimizes Y_i is selected as the optimal solution

$$i_{final} = i \in max(Y_i), i = 1, \cdots, m. \tag{22}$$

5.5.3. *Optimization of grinding process parameters based on wear indicators*

In the industrial manufacturing process, the friction and wear performance is important for the actual application of the SiCp/Al composite. Friction coefficient, wear height and equivalent wear section area are important indicators. Considering the grinding time and energy consumption, the grinding efficiency should be as higher as possible. Some constraint conditions should be considered, to balance the friction and wear performance and grinding efficiency. For the grinding process parameters, the constraint conditions are:

$$\begin{cases} 15\ \mathrm{m/s} < v_s < 35\mathrm{m/s} \\ 0.3\ \mathrm{m}/min < v_s < 0.9\mathrm{m}/min \\ 5\mu\mathrm{m} < a_p < 15\mu\mathrm{m} \end{cases}. \tag{23}$$

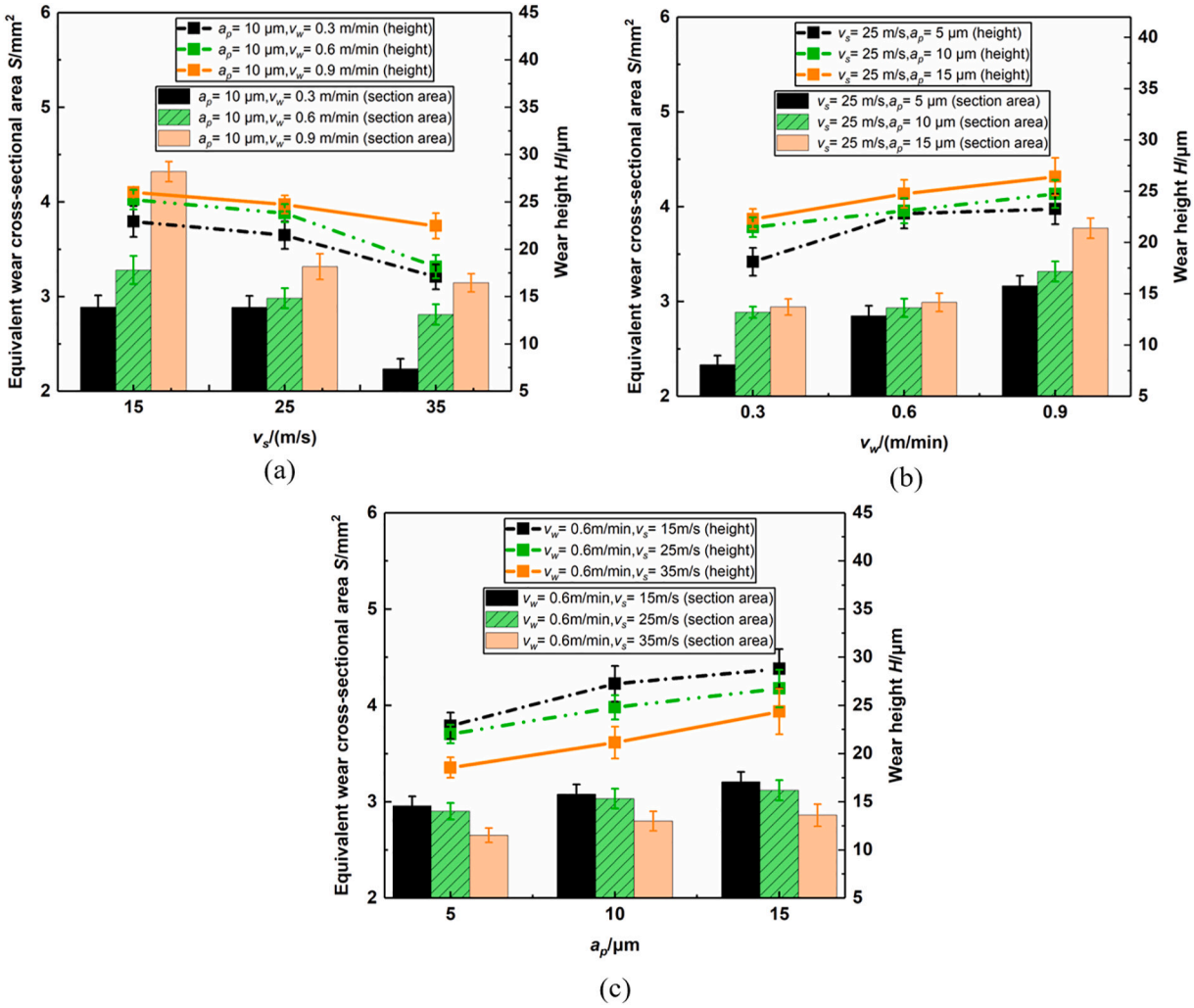

Fig. 15. Relationship between wear height and equivalent wear cross-sectional area and grinding process parameters of SiCp/Al composite ((a) v_s and a_p (b) v_s and v_w (c) v_w and a_p).

In the grinding process of SiCp/Al composite, b is the thickness of the grinding wheel, and the grinding efficiency Q can be expressed as:

$$Q = ba_p v_w. \tag{24}$$

When the grinding process parameters are within this range, the normalized function of grinding efficiency Q is:

$$1 \Big/ Q^{'} = \frac{1/Q - 1/Q_{\max}}{1/Q_{\min} - 1/Q_{\max}}. \tag{25}$$

Based on the prediction model of wear indicators of SiCp/Al composite in Eqs. (15), (16) and (17), the normalized function of wear indicators are:

$$\mu = \frac{\mu - \mu_{\min}}{\mu_{\max} - \mu_{\min}}, \tag{26}$$

$$H^{'} = \frac{H - H_{\min}}{H_{\max} - H_{\min}}, \tag{27}$$

$$S^{'} = \frac{S - S_{\min}}{S_{\max} - S_{\min}}. \tag{28}$$

For the equivalent wear section area and wear height, the hybrid function is established to reflect wear degree, which is shown in Eq. (29):

$$W^{'} = 0.5H^{'} + 0.5S^{'}. \tag{29}$$

The non-dominated sorting algorithm (NSGA-II) was used to optimize the grinding process parameters of SiCp/Al composite. The three target function is Eqs. (26), (27) and (29) respectively. With the help of the mathematical tool software MATLAB 2019b, the NSGA-II algorithm is used for multi-objective optimization. The related parameter settings are shown in Table 9.

Results of the TOPSIS decision method are shown in Fig. 18. The genetic algorithm computed the best grinding process parameters that ensure the lowest wear indicators and the highest efficiency in the grinding process of SiCp/Al composite. The optimum grinding process parameters are shown in Table 10.

The lowest friction coefficient, the highest grinding efficiency are obtained when wheel speed is 33 m/s, with a table speed of 0.4 m/min and a grinding depth of 9 μm. The optimized grinding parameters are input into the Response Surface prediction model to verify the optimized wear indicators of SiCp/Al composite [30]. It is found that the predicted results are consistent with the experimental results in Table 11, within the acceptable error of the prediction model.

6. Conclusion

(1) The friction and wear tests of alumina-SiCp/Al composite are carried out; the dominant wear mechanism of SiCp/Al composite is the combination of cohesive and abrasive wear.

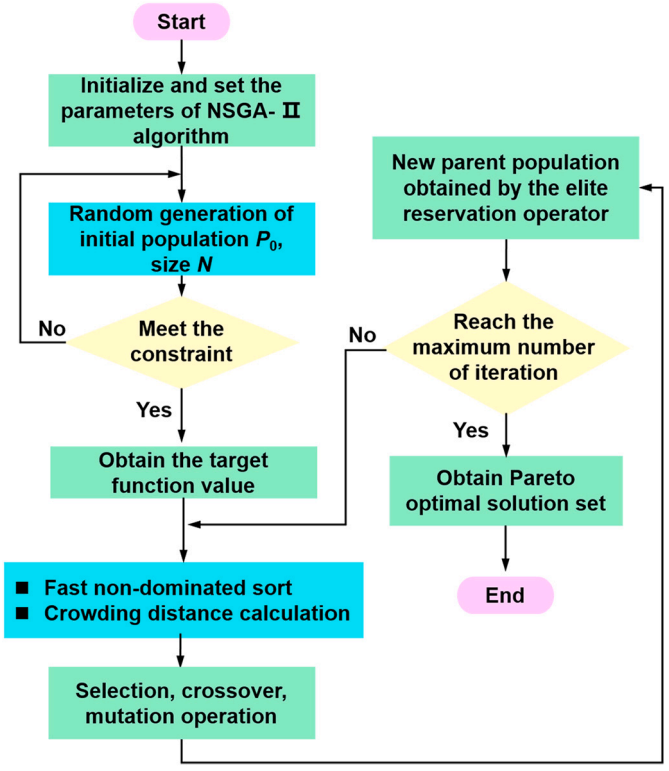

Fig. 16. Specific process of NSGA-II non-dominated sorting genetic algorithm.

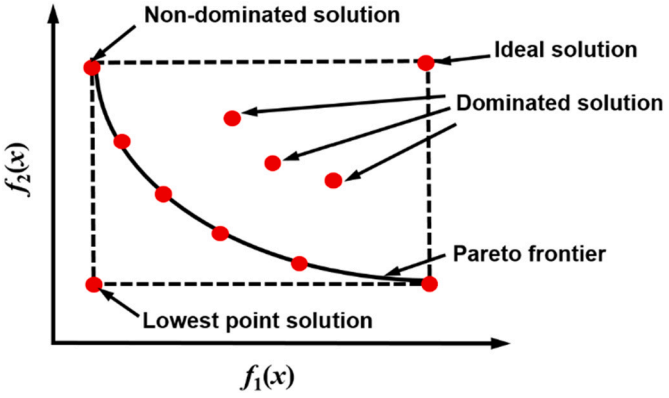

Fig. 17. Distribution of ideal solutions and non-ideal solutions of Pareto front.

Table 9
Table of NSGA-II algorithm parameters.

Parameter name	Set value
Population	600
Connection pool size	200
Maximum number of iterations	500
Cross distribution index	20
Variation Distribution Index	20

(2) A comprehensive evaluation system of SiCp/Al composite is established, in which the three indicators of friction coefficient, wear height, and equivalent wear section area are adopted to evaluate the usability performance.
(3) The comprehensive evaluation system's prediction models of wear indicators were established and verified, and the absolute error between the predicted and experimental results is within 7%.
(4) NSGA-II multi-objective algorithm is adopted to optimize the friction and wear performance of the SiCp/Al composite, the optimized grinding process parameters are obtained as the wheel speed of 33 m/s, the table speed of 0.4 m/min and the grinding depth of 9 μm.

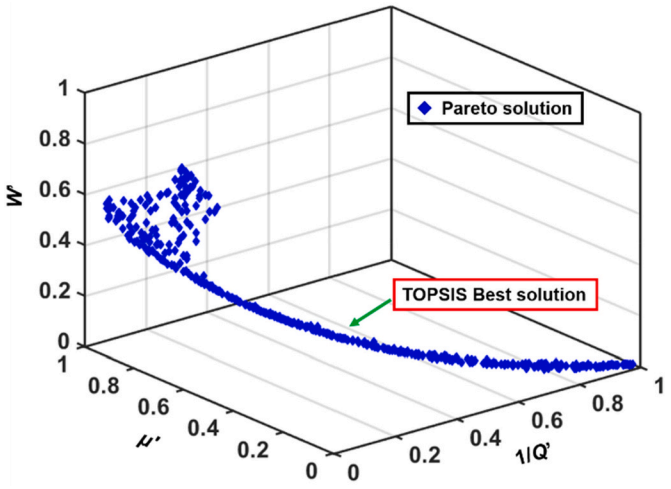

Fig. 18. Prediction convergence of SiCp/Al composite grinding process parameters.

Table 10
Optimized grinding parameters.

Grinding parameters	Optimized results
Wheel speed v_s/m/s	33
Table speed v_w/(m/min)	0.4
Grinding depth a_p/μm	9
Removal rate V/(mm^3/s)	1.8

Table 11
Experimental and predicted results with optimized grinding parameters.

Wear indicators	Experiment results	Predicted results	Error (%)
Friction coefficient μ	0.407	0.392	3.78
Wear height H/mm	19.163	18.367	−4.33
Equivalent wear section area S/mm^2	2.197	2.379	7.65

Declaration of competing interest

All authors of this manuscript have directly participated in planning, execution, and/or analysis of this study. The contents of this manuscript have not been copyrighted or published previously. The contents of this manuscript are not now under consideration for publication elsewhere. The contents of this manuscript will not be copyrighted, submitted, or published elsewhere while acceptance by Journal of Manufacturing Processes is under consideration. There are no directly related manuscripts or abstracts, published or unpublished, by any authors of this manuscript.

Acknowledgement

This work was supported by Science and Technology Program of Shanghai, China (Grant No. 20ZR1462800) and the International Exchange Program for Graduate Students, Tongji University (No.

201902043), thanks for Politecnico di Torino to provide the experimental facilities and help. Giacomo Maculotti would like to thank the support from “Ministero dell'Istruzione, dell'Università e della Ricerca”, Award “TESUN-83486178370409 finanziamento dipartimenti di eccellenza CAP. 1694 TIT. 232 ART. 6”.

References

[1] Mohanty R, Roy M. Thermal sprayed WC-Co coatings for tribological application. Materials and Surface Engineering 2012:121–62. Woodhead Publishing.
[2] Farayibi P, Abioye T, Clare A. A parametric study on laser cladding of ti-6Al-4V wire and WC/W2C powder[J]. Int J Adv Manuf Technol 2016;87:3349–58.
[3] Maculotti G, Senin N, Oyelola O, Galetto M, Clare AT, Leach R. Multi-sensor data fusion for the characterization of laser cladded cermet coatings. In: Proceedings of the Euspen's 19th international conference and exhibition, Bilbao; 2019.
[4] Yin G, Gong Y, Li Y. Modeling and evaluation in grinding of SiCp/Al composites with single diamond grain [J]. Int J Mech Sci 2019:105–37.
[5] Liu J, Cheng K, Ding H. Realization of ductile regime machining in micro-milling SiCp/Al composites and selection of cutting parameters[J]. Proc IME C J Mech Eng Sci 2019;233(12):4336–47.
[6] Zhu C, Gu P, Wu Y. Surface roughness prediction model of SiCp/Al composite in grinding[J]. Int J Mech Sci 2019;155:98–109.
[7] Duan C, Che M, Sun W. Influence of different cooling and lubrication methods on tool wear in machining SiC_P/Al composites[J]. Acta Mater Compos Sin 2019;36 (5):1244–53.
[8] Zhou L, Cui C, Zhang P. Finite element and experimental analysis of machinability during machining of high-volume fraction SiCp/Al composites[J]. Int J Adv Manuf Technol 2017;91(5–8):1935–44.
[9] Zhou M, Wang M, Dong G. Experimental investigation on rotary ultrasonic face grinding of SiCp/Al composites[J]. Mater Manuf Process 2016;31(5):673–8.
[10] Huang S, Zhou L, Yu X. Study of the mechanism of ductile-regime grinding of SiCp/Al composites using finite element simulation[J]. Int J Mater Res 2012;103(10): 1210–7.
[11] Li J, Du J, Yao Y. Experimental study of machinability in mill-grinding of SiCp/Al composites[J]. J Wuhan Univ Technol Mater Sci Ed 2014;29(6):1104–10.
[12] Yin G, Wang D, Jun Cheng. Experimental investigation on micro-grinding of SiCp/Al metal matrix composites[J]. Int J Adv Manuf Technol 2019;102(9–12):3503–17.
[13] Zhou L, Huang S, Yu X. Machining characteristics in cryogenic grinding of SiCp/Al composites[J]. Acta Metall Sin Engl Lett 2014;27(5):869–74.
[14] Du J, Ming W, Cao Y. Particle removal mechanism of high volume fraction SiCp/Al composites by single diamond grit Tool[J]. J Wuhan Univ Technol Mater Sci Ed 2019;34(2):324–31.
[15] Zheng W, Liu L, Zhang Q. Simulation of formation mechanism of machined surface defects in ultrasonic grinding of SiCp/Al composites[J]. J Solid Rocket Technol 2019;42(6):793–800.
[16] Chen Z, Li C, Xu L. Research on the grinding performance of high pressure sintering SiCp/Al matrix composites[J]. Eng Rev 2018;38(2):175–81.
[17] Liang G, Zhou X, Zhao F. The grinding surface characteristics and evaluation of particle-reinforced aluminum silicon carbide[J]. Sci Eng Compos Mater 2016;23 (6):671–6.
[18] Huang S, Yu X, Wang F. A study on chip shape and chip-forming mechanism in grinding of high volume fraction SiC particle reinforced Al-matrix composites[J]. Int J Adv Manuf Technol 2015;80(9–12):1927–32.
[19] Du J, Zhang H, He W. Simulation and experimental study on surface formation mechanism in machining of SiCp/Al composites[J]. Appl Compos Mater 2019;26 (1):29–40.
[20] Ramachandra M, Radhakrishna K. Sliding wear, slurry erosive wear, and corrosive wear of aluminium/SiC composite[J]. Mater Sci-Pol 2006;24(2):333–49.
[21] Dimaki A, Dudkin I, Popov V. Influence of the adhesion force and strain hardening coefficient of the material on the rate of adhesive Wear in a dry tangential frictional Contact[J]. Russian Phys J 2019;62(8):1398–408.
[22] Huang J, Wang M, Li Y. Effect of flake graphite content on wear between behavior between P/M copper-based pantograph slide and contact wire[J]. Mater Res Express 2020;7(7):076510.
[23] Rajeshkumar G. A new study on tribological performance of Phoenix sp. fiber-reinforced epoxy composites[J]. J Nat Fibers 2020. https://doi.org/10.1080/15440478.2020.1724235.
[24] Wang Y, Song J. Dry sliding wear behavior of alumina fiber and SiC particle reinforced aluminium based MMCs fabricated by squeeze casting method[J]. Trans. Nonferrous Met. Soc. China 2011;21:1441–8.
[25] Genta G, Maculotti G. Uncertainty evaluation of small wear measurements on complex technological surfaces by machine vision-aided topographical methods [J]. CIRP Ann 2021;70:451–4.
[26] Maculotti G, Goti E, Genta G, Mazza L, Galetto M. Uncertainty-based comparison of conventional and surface topography-based methods for wear volume evaluation in pin-on-disc tribological test[J]. Tribol Int 2022;165:107260.
[27] Lu B. Fundamentals of machinery manufacturing technology [M]. In: Beijing: China Machine Press; 2007. p. 12.
[28] Zhu C, Gu P, Liu D, et al. Evaluation of surface topography of SiCp/Al composite in grinding[J]. Int J Adv Manuf Technol 2019;102:2807–21.
[29] Montgomery DC. Design and analysis of experiments. 9th ed. New York: Wiley Sons; 2017.
[30] Galetto M, Genta G, Maculotti G, Verna E. Defect probability estimation for hardness-optimised parts by selective laser melting[J]. Int J Precis Eng Manuf 2020;21(9):1739–53.
[31] Xing Y, Yang Y, Xue C. Roughness model of an optical surface in ultrasonic assisted diamond turning. Appl Opt 2020;59(31):9722–34.
[32] Deb K, Pratap A, Agarwal S, et al. A fast and elitist multi-objective genetic algorithm: NSGA-II[J]<icepaste/>. IEEE Trans Evol Comput 2002;6(2):182–97.
[33] Dang G, Su H, Che Y. Research on multi-objective optimization of dish Stirling system based on improved NSGA-II algorithm. J Yunnan Univ Nat Sci Ed 2021;43 (2):270–9.